MINISTRY OF EDUCATION AND TRAINING
HANOI UNIVERSITY OF MINING AND GEOLOGY

TRINH BIEN THUY

RESEARCH ON ROTOR STRUCTURE TO IMPROVE THE OPERATING CHARACTERISTICS OF AN EXPLOSION-PROOF LINE-START PERMANENT MAGNET SYNCHRONOUS MOTOR USED IN UNDERGROUND MINING

Major: Electrical Engineering
Code: 9520201

SUMMARY OF DOCTORAL DISSERTATION IN ENGINEERING

HANOI – 2026

The dissertation was completed at: **Department of Electrical Electrification Faculty of Mechanical and Electrical Engineering Hanoi University of Mining and Geology**

Academic Supervisors:

1. Assoc. Prof. Dr. Do Nhu Y

2. Dr. Le Anh Tuan

Reviewer 1: Assoc. Prof. Dr. Nguyen Kien Trung

Reviewer 2: Dr. Nguyen Thac Khanh

Reviewer 3: Assoc. Prof. Dr. Tran Thanh Son

The dissertation will be defended before the University-level Dissertation Evaluation Council at Hanoi University of Mining and Geology at …… on ………, 2026.

The dissertation can be accessed at:

- The National Library of Vietnam

- The Library of Hanoi University of Mining and Geology

INTRODUCTION

1. Rationale of the Dissertation

Currently, the capacity and depth of mining operations are continuously increasing, resulting in the growing use of machinery and equipment in mining activities to replace human labor. The mechanization of mining processes has led to an increasing demand for electrical energy, causing the proportion of electricity costs per ton of extracted coal to become increasingly significant.

The above solutions have achieved certain effectiveness in promoting energy conservation and efficient energy utilization. However, a large proportion of electricity consumption in mining operations is associated with electric drive systems. In Vietnamese mining operations, electrical energy consumed by electric motors accounts for more than 75% of the total electricity consumption of a mine.

To improve energy efficiency, one potential solution is to replace explosion-proof induction motors (Ex-IM) with explosion-proof line-start permanent magnet synchronous motors (Ex-LSPMSM) directly connected to the power grid. Therefore, the dissertation entitled **"Research on Rotor Structure to Improve the Operating Characteristics of Explosion-Proof Line-Start Permanent Magnet Synchronous Motors Used in Underground Mining"** is of significant necessity and high practical relevance.

2. Objectives of the Dissertation

a. General Objective

To propose an appropriate rotor structure for converting an explosion-proof induction motor (Ex-IM) into an explosion-proof line-start permanent magnet synchronous motor (Ex-LSPMSM) with improved operating characteristics and high efficiency.

b. Specific Objectives

- Successfully convert an Ex-IM with a 160 mm shaft center height into an Ex-LSPMSM.

- Improve the operating parameters, including the starting characteristics and current characteristics of the Ex-LSPMSM, while ensuring that the designed motor efficiency is maintained.

- Minimize manufacturing costs through the appropriate selection of permanent magnets used in the Ex-LSPMSM.

3. Novelty and Contributions of the Research

* Scientific Contributions

- A rotor structure with three permanent magnet bars without magnetic bridges is proposed for the 160 mm shaft center height, 3,000 rpm Ex-LSPMSM, which is suitable for local ventilation fans and water pumps in underground mining applications.

- The influence of the starting current on the demagnetization phenomenon of permanent magnets during the starting process is analyzed and evaluated.

- Appropriate permanent magnet parameters are selected for the 160 mm shaft center height, 3,000 rpm Ex-LSPMSM to improve its operating characteristics while considering the demagnetization conditions.

* Practical Contributions

A 15 kW Ex-IM is successfully converted into a 15 kW - 3,000 rpm Ex-LSPMSM with operating characteristics suitable for ventilation fan and water pump loads in underground mining applications, thereby improving electrical energy utilization efficiency. The proposed technical solution provides useful references for designers and manufacturers in gradually improving and applying Ex-LSPMSM motors in mining operations.

4. Research Object and Scope

- The research object is an Ex-LSPMSM with a 160 mm shaft center height and a speed of 3,000 rpm, which is converted from an Ex-IM with the same technical specifications (rated power of 15 kW, number of pole pairs 2p = 2) and the same shaft center height of 160 mm.

- The research scope of the dissertation: The dissertation focuses on investigating the design of rotor structure and permanent magnet dimensions in the motor rotor, while the remaining motor parameters are maintained unchanged.

5. Research Contents

- Overview of the research problem
- Mathematical modeling of the Ex-LSPMSM
- Determination of rotor structure to improve the operating characteristics of the Ex-LSPMSM
- Experimental investigation and evaluation of results

6. Research Methodology

To achieve the objectives of the dissertation, the following research methods are employed:

- Theoretical research methods;
- Finite Element Method (FEM)-based simulation;
- Experimental methods.

7. Novel Contributions of the Dissertation

- A rotor structure with three permanent magnet bars without magnetic bridges is proposed for the 160 mm shaft center height, 3,000 rpm Ex-LSPMSM, which is suitable for local ventilation fans and water pumps in underground mining applications.
- Appropriate permanent magnet parameters are selected for the 160 mm shaft center height, 3,000 rpm Ex-LSPMSM to improve its operating characteristics while considering the demagnetization conditions.
- A 15 kW, 3,000 rpm Ex-LSPMSM prototype is successfully manufactured and experimentally tested in a laboratory environment for application to local ventilation fan and water pump loads in underground mining operations.

CHAPTER 1.OVERVIEW OF THE RESEARCH PROBLEM

1.1. Overview of Ex-LSPMSM

An explosion-proof line-start permanent magnet synchronous motor (Ex-LSPMSM) is an integration of a line-start permanent magnet synchronous motor (LSPMSM) [9] with an explosion-proof enclosure (Ex), allowing the motor to operate safely in hazardous environments such as underground mining areas with risks of fire and explosion.

1.1.1. Structure of Ex-LSPMSM

The Ex-LSPMSM is a combination of an interior permanent magnet synchronous motor (IPMSM) and a squirrel-cage induction motor [10]. The structure of the Ex-LSPMSM integrates the characteristics of both motor types to maximize their advantages in practical operation [73].

1.1.2. Operating Characteristics of Ex-LSPMSM

1.1.3. Applications of LSPMSM in Underground Coal Mining

In underground coal mining operations, a significant proportion of electrical energy consumption is concentrated in explosion-proof electric drive systems. Statistical results show that the loads among underground coal mining loads, mine ventilation fans account for the largest proportion of electrical energy consumption, representing approximately 32.95% of the total electricity consumption. They are followed by other major load groups, including transportation systems, mine development, coal screening and processing systems, and auxiliary consumption loads [3].

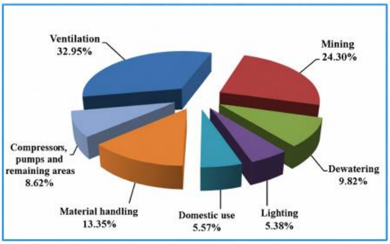

Figure 1.8. Distribution of electrical energy consumption in different mining processes.

1.2. Overview of Research on LSPMSM Structures

1.2.1. Overview of Domestic Research

- Nguyen Vu Thanh (2015) [13] focused on investigating the design algorithm and complete manufacturing process of a three-phase line-start permanent magnet synchronous motor (LSPMSM) directly connected to the power grid.

- Le Anh Tuan [9] developed a mathematical model and simulated the starting characteristics of an LSPMSM considering magnetic circuit saturation and skin effect for a 2.2 kW, 1,500 rpm motor.

- Bui Minh Dinh [2] studied and mastered the calculation, design, and manufacturing technology of a series of LSPMSMs up to 11 kW, 1,500 rpm, achieving IE2 efficiency class according to IEC 60034-30.

In general, domestic studies have established an important foundation for modeling, design, and manufacturing of LSPMSMs. However, these studies have mainly focused on lower power ranges and lower speed applications, and have not yet deeply investigated 15 kW, 3,000 rpm explosion-proof LSPMSMs for underground mining applications.

1.2.2. Overview of International Research

a. Research on Permanent Magnet Arrangement Structures

Regarding this research direction, several studies have been conducted. Reference [64] investigated the rotor structure of a 3.7 kW LSPMSM. The authors proposed a rotor structure using three permanent magnet bars arranged inside the rotor. Reference [37] presented a novel structure of a two-pole, 37 kW LSPMSM operating at 3,000 rpm (50/60 Hz). Reference [28] designed a permanent magnet rotor structure with a fan-shaped arrangement...

b. Research on Factors Affecting the Operating Parameters of LSPMSM

Due to the significant advantages of LSPMSMs, the design and development of this type of motor have attracted considerable attention from researchers worldwide. Reference [78] performed optimal design calculations for LSPMSMs based on electromagnetic and thermal analyses. Reference [21] investigated improvements in torque characteristics, starting capability, and steady-state operating performance of LSPMSMs. Reference [20] studied the starting process and mathematical modeling of LSPMSMs. Reference [82] conducted a comparison between induction motors (IMs) and line-start permanent magnet synchronous motors (LSPMSMs) based on the d–q model of both types of machines. Reference [69] analyzed demagnetization in a 1,500 rpm LSPMSM and proposed solutions to reduce the demagnetization phenomenon...

c. Research on Solutions for Optimizing LSPMSM Parameters

Several studies have been conducted in this research direction. Reference [79] presented an analytical method and design optimization approach for line-start permanent magnet synchronous motors (LSPMSMs). Reference [95] proposed a design procedure for LSPMSMs, including the selection of basic dimensions similar to those used for induction motors (IMs), with a squirrel-cage rotor structure integrated with fan-shaped permanent magnets. Reference [28] focused on improving the efficiency and power factor of a 7.5 kW LSPMSM through rotor structure optimization. Reference [68] focused on optimizing permanent magnet dimensions to reduce the manufacturing cost of LSPMSMs...

Table 1.3. Comparison of the Dissertation Contributions with Typical Research Directions on LSPMSMs

Criteria	Previous Studies	This Dissertation
Research object	Mainly focused on LSPMSMs for conventional industrial applications.	Ex-LSPMSM used for local ventilation fans and water pumps in underground mining applications.
Power and speed range	Mostly concentrated on low- or medium-power motors; many studies	Investigated a 15 kW, 3,000 rpm Ex-LSPMSM.

	investigated motors operating at 1,500 rpm.	
Rotor structure and demagnetization	Mainly investigated individual rotor configurations or permanent magnet arrangements; limited analysis of demagnetization associated with specific application conditions.	Proposed a rotor structure with three permanent magnet bars without magnetic bridges; analyzed the influence of starting current on demagnetization and selected NdFeB N38 permanent magnets.

1.3. Research Gap

Based on the above analyses, it can be observed that the main research gap lies in the problem of selecting an appropriate rotor structure for medium-power, high-speed Ex-LSPMSMs capable of operating in underground mining conditions. Accordingly, this dissertation focuses on investigating rotor structure solutions for converting an Ex-IM with a 160 mm shaft center height and a speed of 3,000 rpm into an Ex-LSPMSM suitable for ventilation fan and water pump loads in underground mining applications. The research not only aims to improve the motor efficiency but also focuses on clarifying the influence of rotor structure and permanent magnet parameters on the starting characteristics, current quality, synchronization capability, and operational reliability of the motor.

1.4. Conclusions

- The LSPMSM is a hybrid motor combining the advantages of both the induction motor (IM) and the permanent magnet synchronous motor (PMSM). It can achieve direct line starting due to the squirrel-cage structure embedded in the rotor, while operating continuously at synchronous speed in the steady state, resulting in the elimination of rotor copper losses and improvement of motor efficiency. Therefore, the LSPMSM is classified as a high-efficiency and ultra-high-efficiency motor. However, the main disadvantage of this motor type is its low starting torque.

- With the current trend toward energy conservation and efficient energy utilization, the Ex-LSPMSM is gradually replacing Ex-IMs in some applications with suitable operating conditions, such as ventilation fans and drainage pumps.

- Previous studies on LSPMSMs have mainly focused on two research directions: optimal design of LSPMSMs from the initial design stage or conversion of IMs into LSPMSMs. Most studies have been conducted on LSPMSMs with low power ratings below 7.5 kW and speeds of 1,500 rpm. No studies have been reported on motors in the 11 kW–18.5 kW power range and 3,000 rpm speed, particularly motors with a 160 mm shaft center height and one pair of poles, which are widely used for ventilation fan and local water pump loads in underground mining operations.

Based on the above issues, this dissertation focuses on investigating an appropriate rotor structure for converting a 160 mm shaft center height, 3,000 rpm Ex-IM into an Ex-LSPMSM suitable for local water pumps and ventilation fans in underground mining applications.

The research tasks include analyzing the permanent magnet arrangement structure and determining the permanent magnet dimensions and parameters to improve the starting characteristics, torque performance, current characteristics, and back electromotive force (Back-EMF) of the Ex-LSPMSM.

CHAPTER 2. MATHEMATICAL MODEL OF LSPMSM

2.1. Mathematical Model of LSPMSM

The Ex-LSPMSM model proposed by Honsinger [83].

$$\begin{cases} u_d = r_1 i_d + \frac{d\Psi_d}{dt} - \omega_r.\Psi_q \\ u_q = r_1 i_q + \frac{d\Psi_q}{dt} + \omega_r.\Psi_d \\ 0 = r'_d i'_d + \frac{d\Psi'_d}{dt} \\ 0 = r'_q i'_q + \frac{d\Psi'_q}{dt} \\ Te = \frac{m}{2}.p.\left(\Psi_d i_d - \Psi_q i_q\right) \end{cases} \quad (2.1)$$

If the motor is excited solely by permanent magnets

$$\begin{cases} \Psi_d = L_d i_d + L_{md} i_{2d} + \Psi_m \\ \Psi_q = L_q i_q + L_{mq} i_{2q} \\ \Psi_{2d} = L_{2d} i_{2d} + L_{md} i_d + \Psi_m \\ \Psi_{2q} = L_{2q} i_{2q} + L_{mq} i_q \end{cases} \quad (2.2)$$

Voltage Equations of the Ex-LSPMSM Based on Honsinger's Model [83].

Stator Voltage
$$\begin{cases} u_{ds} = r_1 i_{ds} + \frac{d\Psi_{ds}}{dt} - \omega_r.\Psi_{qs} \\ u_{qs} = r_1 i_{qs} + \frac{d\Psi_{qs}}{dt} + \omega_r.\Psi_{ds} \end{cases} \quad (2.3)$$

Rotor voltage
$$\begin{cases} u'_{dr} = r'_{dr} i'_{dr} + \frac{d\Psi'_{dr}}{dt} = 0 \\ u'_{qr} = r'_{qr} i'_{qr} + \frac{d\Psi'_{qr}}{dt} = 0 \end{cases} \quad (2.4)$$

Stator Flux
$$\begin{cases} \Psi_{ds} = (L_{ls} + L_{md}) i_{ds} + L_{md} i'_{dr} + \Psi'_m \\ \Psi_{qs} = (L_{ls} + L_{mq}) i_{qs} + L_{mq} i'_{qr} \end{cases} \quad (2.5)$$

Rotor flux
$$\begin{cases} \Psi'_{dr} = L'_{lr} i'_{dr} + L_{md}(i_{ds} + i'_{dr}) + \Psi'_m \\ \Psi'_{qr} = L'_{lr} i'_{qr} + L_{mq}(i_{qs} + i'_{qr}) \end{cases} \quad (2.6)$$

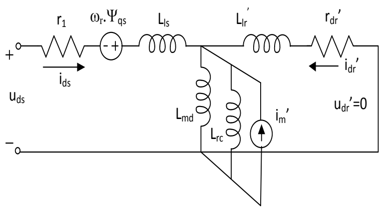

Figure. 2.1. Equivalent circuit diagram of the d-axis of the Ex-LSPMSM [83]

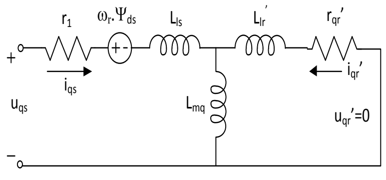

Figure. 2.2. Equivalent circuit diagram of the q-axis of the Ex-LSPMSM [83]

The electromagnetic torque equation of the Ex-LSPMSM is expressed as follows: [25]

$$M_{dt} = \frac{3}{2}.p.\left[\underbrace{\left(L_{md}.i'_{dr}.i_{qs} - L_{mq}.i'_{qr}.i_{ds}\right)} + \underbrace{\Psi'_{m}.i_{qs}} + \underbrace{(L_{md} - L_{mq}).i_{ds}.i_{qs}}\right] \quad (2.7)$$

Electromagnetic Torque: $T_e = T_{ind} + T_{PM} + T_{rel}$ (2.8)

2.2. Modeling of Ex-LSPMSM Using the Finite Element Method

2.2.1. Finite Element Method (FEM)

For an electric motor operating under steady-state conditions, the Maxwell–Faraday equation is expressed as follows: [5],[7].

$$\nabla.\vec{H} = \vec{J} \quad (2.10)$$

The magnetic field strength $\vec{H}$ is related to the magnetic flux density $\vec{B}$ by the following expression:

$$\vec{B} = \mu_0\mu_r\vec{H} \quad (2.11)$$

In the electromagnetic field, $\vec{B}$ is calculated through the magnetic vector potential $\vec{A}$ as follows:

$$\vec{B} = \nabla.\vec{A} \quad (2.12)$$

The equation that results from replacing ((2.11) and (2.12)) in equa tion (2.10) is as follows

$$\nabla \times \left(\frac{1}{\mu_0\mu_r}\nabla.\vec{A}\right) = \vec{J} \quad (2.13)$$

Poisson's equation, which has the general form given by equation (2.13), can be understood as follows in the analytical model corresponding to the Oxyz coordinate system:

$$\frac{1}{\mu_0\mu_r}\left(\frac{\partial^2 A}{\partial x^2} + \frac{\partial^2 A}{\partial y^2} + \frac{\partial^2 A}{\partial z^2}\right) + J = 0 \quad (2.14)$$

The magnetic potential vector A (2.14) can be found through (10). Utilizing the solutions to equations ((2.11) and (2.12)) compute the mag netic flux density B and magnetic field intensity H as follows:

$$\vec{B} = B_x\vec{i} + B_y\vec{j} + B_z\vec{k} = \left(\frac{\partial A_z}{\partial y} - \frac{\partial A_y}{\partial z}\right)\vec{i} + \left(\frac{\partial A_x}{\partial z} - \frac{\partial A_z}{\partial x}\right)\vec{j} + \left(\frac{\partial A_y}{\partial x} - \frac{\partial A_x}{\partial y}\right)\vec{k} \quad (2.15)$$

The following equations can be used to calculate the DC cur rent of the coil and the voltage applied to its two coil terminals:

$$U = R_{dc} i + L\frac{di}{dt};\ I_{dc} = \frac{U}{R_{dc}} \quad (2.16)$$

2.2.2. Common FEM Software Used in Electrical Machine Research

2.2.3. FEM-Based Modeling of LSPMSM Using Simulation Software

The Ex-LSPMSM has the following specifications: rated power of 15 kW, speed of 3,000 rpm, and its dimensions are provided in Table 2.1. [10]:

Table 2.1. Specifications of the 15 kW, 3,000 rpm Ex-LSPMSM

Parameter	***Symbol***	***Value***	***Unit***
Stator outer diameter	D_{out}	245	mm
Stator inner diameter	D_{in}	152	mm
Rotor outer diameter	D’	151	mm
Rotor shaft diameter	Dt	52	mm
Stator steel material	Steel 1008		
Number of stator slots	Z_1	36	slot
Number of rotor slots	Z_2	28	slot
Air gap length	δ	0,5	mm
Supply voltage	U_n	380/660	V
Frequency	f	50	Hz
PM Grade	NdFeB	N38SH	
Bar dimensions (length x width x thickness)	mm	35.34.8	

The preliminary sizing of permanent magnets in Ex-LSPMSMs is typically carried out according to the following steps [5]:

- Preliminary calculation and selection of the maximum magnet width W_m:

$$W_{max} = \sqrt{2}R_{1max} \quad (2.17)$$

- Calculate the minimum volume of the magnet used

$$V_m = \frac{2.k_{ocf}.k_{fd}.(1+k_{EC}).P_{đm}}{\pi^2.\xi.2.p.f.B_r.H_c} \quad (2.18)$$

Based on the magnet volume V_m and the maximum width b_{max} determined above, the minimum thickness of the magnet can be calculated h_{min}:

$$h_{min} = \frac{V_m}{H_m . b_{max}} \tag{2.19}$$

* Note: Preliminary calculations for the 15 kW Ex-LSPMSM yielded the magnet thickness h_{min} = 7,3 mm, b_{max} = 34 mm. Investigation of the operating characteristics of the Ex-LSPMSM n = 3.000 rpm, $P_{đm}$ = 15 kW, $U_{đm}$ =380/660V, Use permanent magnet type N=38 with preliminary selected magnet thickness: h = 7 mm. In order to study the characteristics of Ex-LSPMSM, the author uses finite element method (FEM) software to simulate LSPMSM. The simulation results are intended to study and evaluate the design of the engine.

2.3. Analysis of rotor structural design using the finite element method

2.3.1. Selecting the magnet shape

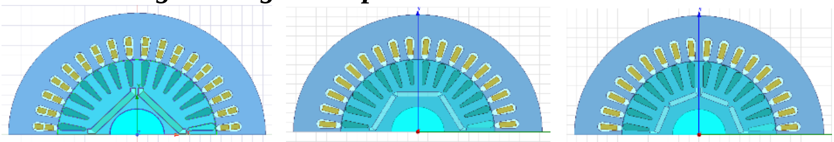

a) Divide into 2 bars b) Divide into 3 bars c) Divide into 4 bars

Figure 2.6. LSPMSM configuration – 2-pole.

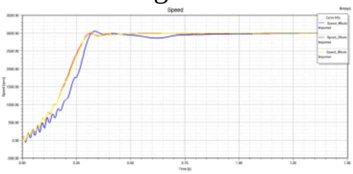

Figure 2.8. Startup speed curves for 2-, 3-, and 4-bar configurations.

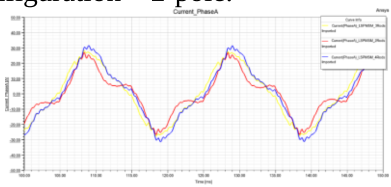

Figure 2.9. Steady-state current curve.

Table 2.4. THDi calculation results.

Parameter	[17]	Two-bar configuration	Three-bar configuration	Four-bar configuration
THDi	≤20%	26,6%	18,8%	24,5%

* Observation: The results in Table 2.4 show that the 3-magnet configuration yields the lowest THDi value (18.8%), while the 2-magnet configuration yields the highest. Both the 2-magnet and 4-magnet configurations exceed the specified harmonic requirements [17]. It is concluded that the 3-magnet configuration is the optimal choice.

2.3.2. Rotor configuration selection for LSPMSM

2.3.2.1. Analytical model for determining air-gap magnetic flux

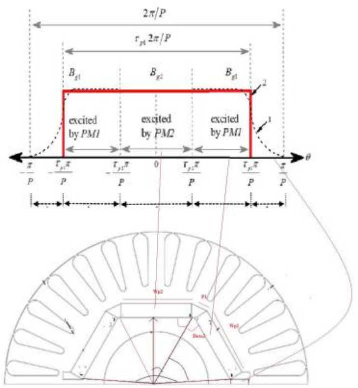

Figure 2.13. Equivalent model of air-gap magnetic flux density distribution

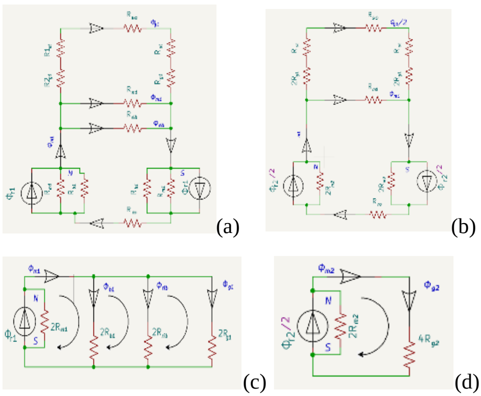

Figure 2.14. Magnetic circuit models based on the stacking method

a), (b) Model based on PM1; (c), (d) Model based on PM2.

Based on Figure 2.14, the following mathematical expressions can be formulated: $\emptyset_{r1} = B_r A_{p1} = B_r L_{stk} w_{p1}$ (2.21)

$$\emptyset_{r2} = B_r A_{p2} = B_r L_{stk} w_{p2} \quad (2.22)$$

The various reluctance parameters and the air gap area can be expressed as follows:

$$R_{g1} = \frac{g_o}{\mu_o A_{g1}} \quad (2.23)$$

$$R_{g2} = \frac{g_o}{\mu_o A_{g2}} \quad (2.24)$$

Based on the rotor shape of the Ex-LSPMSM motor, the magnetic pole arc angle (θ□) determined based on the permanent magnet segments within each pole, the effective air gap area is expressed by the following formula [27]:

$$\frac{\theta_m}{2} = (\theta_{m1} + \theta_{m2}) \tag{2.31}$$

$$\alpha_m = \theta_a + \theta_b; \hat{\mathrm{O}}\mathrm{m} = \theta_c + \theta_d \tag{2.32}$$

$$A_g = A_{g1} + A_{g2} \tag{2.33}$$

The leakage flux in the bridges can be estimated using the following formula [27]: $\emptyset_{bri} \approx B_{sat}A_{bri}$ (2.39)

The equivalent magnetic flux distribution model demonstrates that the air-gap magnetic flux density distribution along the rotor radius, as determined by the analytical model, shows significant agreement with results obtained from finite element method (FEM) simulations. Therefore, it can be assumed that these two sets of results are equivalent. $B_{g1} \approx B_{g2} = B_g$ (2.52)

$$B_g\left(L_{gp}, \alpha_m\right) = \frac{B_{r1}A_{m1}}{A_{g1}[1+\gamma(1+\alpha+\beta)]} \approx \frac{B_{r2}A_{m2}R_{m2}}{A_{g2}(R_{g2}+R_{m2})} \tag{2.53}$$

Với $\gamma = 0{,}31; \alpha = 0{,}55; \beta = 1{,}58; B_{r1} = 1{,}23T; \frac{Am}{Ag} = 1 \rightarrow B_g = 0{,}624(T)$

2.3.2.2. FEM model for determining air-gap magnetic flux

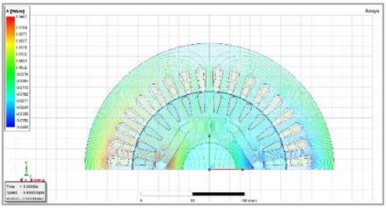

Figure 2.16. Magnetic field distribution in a motor without a magnetic bridge

Table 2.5. Comparison of air-gap magnetic flux density and no-load electromotive force between design reference values and FEM simulation results

Parameter	Analytical Calculation	FEM Simulation	Error E%
B_g(T)	0,624	0,59	4,8
E_{1NB} (V)	380	395	3,8

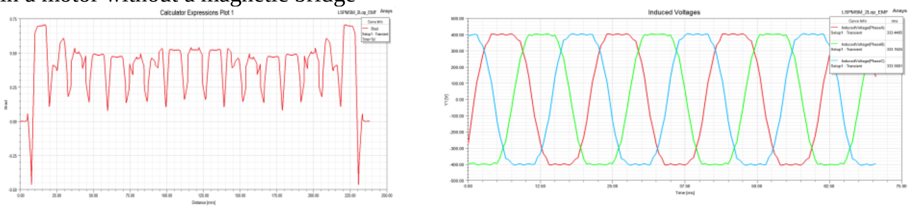

Figure 2.17. Air-gap magnetic flux (a) and no-load back-EMF (b)

* Observation: The discrepancy between the analytical model and the FEM simulation is less than 5%, indicating that the finite element model developed in Ansys/Maxwell is reliable and consistent with the analytical model. Therefore, the FEM model will be used in the dissertation to study the Ex-LSPMSM, replacing the analytical model.

2.3.2.3. Selection of the permanent magnet slot configuration

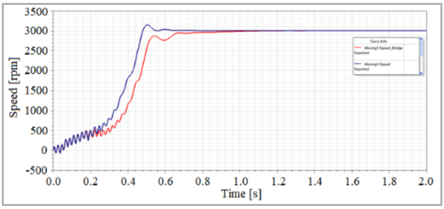

Figure 2.19. Starting characteristics of the motor

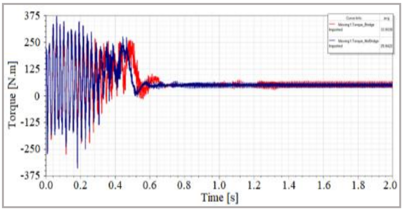

Figure 2.20. Torque characteristics of the motor

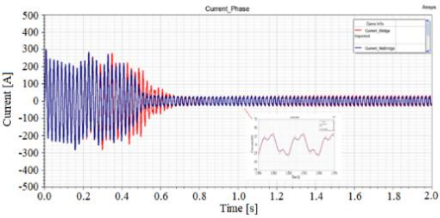

Figure 2.21. Current characteristics in steady-state operation

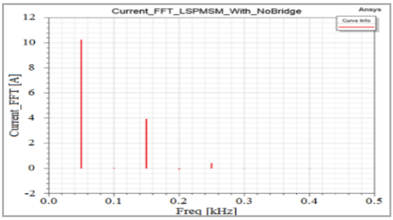

Figure 2.22. FFT analysis of current harmonics

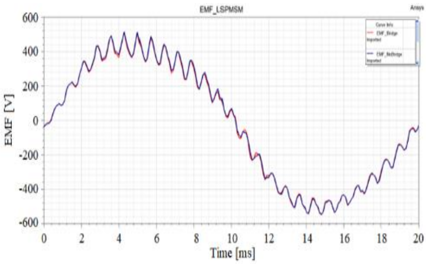

Figure 2.23. No-load electromotive force characteristic.

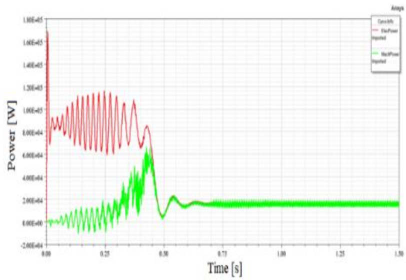

Figure 2.24. Electromagnetic power and mechanical power during the Ex-LSPMSM simulation

*Observation: Simulations using Ansys/Maxwell software indicate that a rotor configuration without magnetic bridges enables the Ex-LSPMSM to achieve superior operating parameters. This structure was selected for fabrication and experimental evaluation.

2.4. Conclusions

Chapter 2 developed and comprehensively analyzed the mathematical model of the Ex-LSPMSM, establishing the theoretical foundation and simulation tools for the design and experimental work in subsequent chapters.

The mathematical model accounts for three characteristic torque components: asynchronous torque during the starting phase, permanent magnet excitation torque, and reluctance torque.

The Finite Element Method (FEM) was applied using ANSYS/Maxwell software to simulate the magnetic field distribution, electromagnetic torque, and starting characteristics of the motor. A comparison between the analytical and numerical models yielded an error of less than 5%, demonstrating the high accuracy and reliability of the proposed simulation method.

Based on the FEM model, the dissertation investigated various rotor structural designs—varying the number and arrangement of magnet bars (2, 3, and 4 bars) and assessing the impact of magnetic bridges. The results indicate that the three-magnet-bar rotor configuration without magnetic bridges is optimal, offering a short synchronization time (t_s = 0.45 s), low torque ripple (RipT = 23.1%), low total harmonic distortion of current (THDi = 14.3%), and high efficiency (η = 93.3%). This configuration minimizes leakage flux, increases starting torque, and improves overall electromagnetic performance.

Thus, Chapter 2 established a reliable theoretical foundation and simulation toolkit for the rotor design of the Ex-LSPMSM, confirming the feasibility and effectiveness of combining mathematical modeling with finite element analysis in the research and development of Ex-

LSPMSM motors. These results serve as the basis for selecting rotor structural parameters in Chapter 3.

CHAPTER 3. ANALYSIS OF ROTOR STRUCTURAL PARAMETER SELECTION FOR LSPMSM

3.1. Demagnetization of permanent magnets

3.1.1. Permanent magnet

3.1.2. Analysis of the demagnetization process of permanent magnets

To model the demagnetization phenomenon of a magnet, it is necessary to establish the relationship between B, H, and M for the magnetic material. This relationship is described by the B–H curve.

$$B = \mu_0(H + M) \tag{3.2}$$

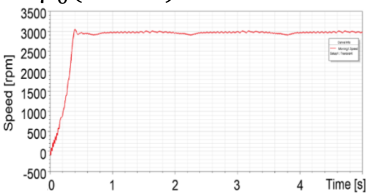

Figure 3.8. Speed characteristics of a motor with asymmetrical partial demagnetization.

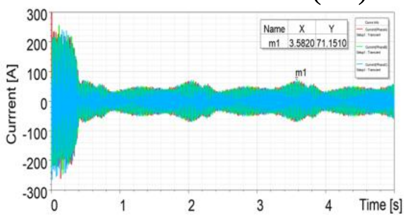

Figure 3.9. Current characteristics of a partially demagnetized motor.

* Observation: Simulation results indicate that during the starting process of the 3-bar Ex-LSPMSM, the two outer bars are the most susceptible to demagnetization, and the degree of demagnetization varies among the bars.

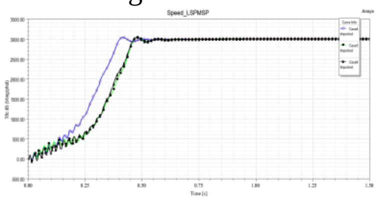

Figure 3.13. Speed characteristics of the Ex-LSPMSM under flux weakening with two symmetrically positioned PM pairs

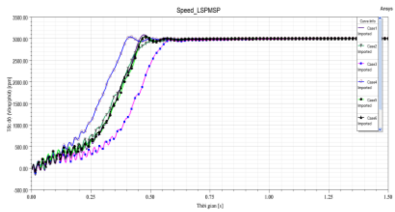

Figure 3.14. Speed characteristics of the Ex-LSPMSM under flux weakening, with one and two pairs of symmetrically arranged PM.

Table 3.3. Performance of the Ex-LSPMSM under flux weakening with a symmetrical pair of PM

No.	Efficiency η(%)	No.	Efficiency η(%)
Case 1	91,2	Case 4	90,2
Case 2	92,8	Case 5	92,5
Case 3	93,3	Case 6	92,8

* Observation: From Table 3.3, it can be seen that Case 3 yields the highest efficiency (93.3%) but has the poorest starting characteristics. Conversely, Case 4 exhibits the best starting characteristics but the lowest efficiency (90.2%)

3.1.3. Conditions for ensuring demagnetization resistance of the PM LSPMSM

It is crucial to calculate and design the rotor structure to prevent demagnetization during the startup of the Ex-LSPMSM. Two types of demagnetization curves are commonly used, wherein the magnetic flux density in the magnet is expressed as a function of the magnetic field (B-H curve). The worst-case scenario for irreversible demagnetization occurs when all magnetomotive forces (MMFs) act in opposition to the direction of F_{pm}. The total magnetomotive force F is determined by the combination of the four MMFs—F_s, F_r, F_g, and F_{pm}—as follows [34]:

$$F = F_{pm} + F_s + F_r + F_g \quad (3.9)$$

To avoid the irreversible demagnetization analyzed above, the thickness of the permanent magnet must satisfy the following formula [34]:

$$I \leq l_M \frac{2}{m}.\frac{\pi}{4}.\frac{2.p.H_C}{\sqrt{2}.N.k_w} \quad (3.13)$$

$$I.\frac{m}{2}.\frac{4}{\pi}.\frac{\sqrt{2}.N.k_w}{2.p.H_C} \leq l_M \quad (3.14)$$

3.2. Analysis of parameter selection for permanent magnets

3.2.1. Parametric analysis method

3.2.2. Analysis and Selection of Permanent Magnet type:

$$V_M = \frac{2k_{of}(1+k_{EC})P_2}{\pi^2 \xi 2pfB_rH_C} \quad (3.27)$$

$$l_M \geq \frac{m}{2}\frac{4}{\pi}\frac{\sqrt{2}Nk_{ws}}{2pH_C}I_p \quad (3.28)$$

With the 15 kW Ex-LSPMSM motor, the research has: m = 3; k_{ws} = 0,92; N = 120 turns/phase; HC = 950000 A/m; I = 26,2 A → I_P = 2,2.26,2 = 57,6 (A)

$$\rightarrow l_M \geq \frac{3}{2}\frac{4}{3{,}14}\frac{\sqrt{2}.120.0{,}92}{2.950000}.57{,}6 = 9\,mm \ \rightarrow choose\ l_M = 9\,mm$$

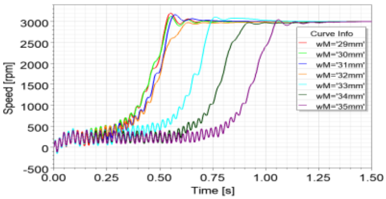

Figure 3.20. Starting speed characteristics of the Ex-LSPMSM 15 kW, 2p = 2

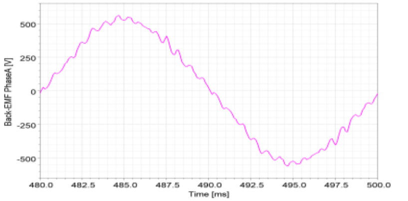

Figure 3.25. Back-EMF waveform of the 15 kW, 2p=2 Ex-LSPMSM with W_M = 35 mm

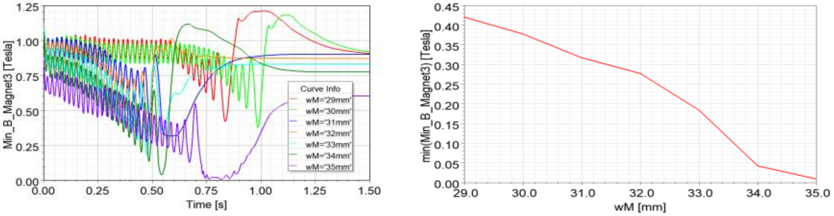

Figure 3.23. Global minimum of the operating state of PM3

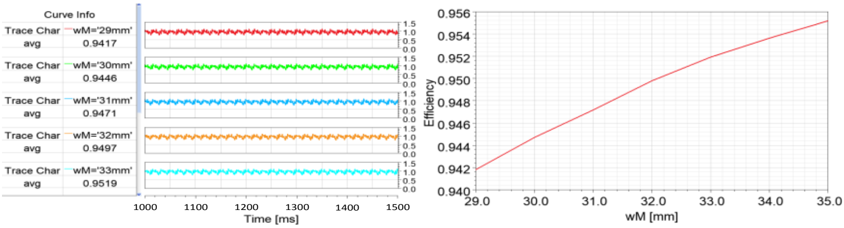

Figure 3.26. Steady-state performance characteristics of the Ex-LSPMSM

Table 3.8. Performance of the Ex-LSPMSM under steady-state operation

W_M (mm)	**Efficiency η**	**W_M (mm)**	**Efficiency η**
29	0.9417	33	0.9519
30	0.9446	34	0.9536
31	0.9471	35	0.9551
32	0.9497		

* Observation: The above analysis indicates that, to ensure operational parameters and avoid the risk of demagnetization during startup, one can select PM dimensions with a thickness of 9 mm and a width of 33 mm for high starting current multiples, or a width of 34 mm for low starting current multiples (ensuring the load characteristic curve does not shift to the left of the I/4 corner); this maintains motor efficiency at 95.19% or 95.36%, respectively.

3.3. Analysis and evaluation for selecting the PM type

3.3.1. Magnetic flux density in the air gap produced by the PM

The magnetic circuit parameters under no-load conditions are determined:

$$\Lambda_t = \Lambda_\delta + \Lambda_\sigma = k_{\sigma M}.\Lambda_\delta \quad (3.39)$$

The magnetic permeability of PM is determined:

$$\Lambda_M = \frac{\mu_0 \mu_{rec} S_M}{h_m} \quad (3.40)$$

Thus, the air-gap magnetic flux is determined:

$$\Phi_{\delta 0} = \frac{\Lambda_\delta}{\Lambda_M / k_{\sigma M} + \Lambda_\delta} \Phi_{rem} \quad (3.41)$$

The air-gap flux under no-load conditions is determined:

$$\Phi_{\delta 0} = \frac{\Phi_{rem}}{k_{\sigma M} + \mu_{rec} k_C \frac{C_\Phi}{C_p}} \quad (3.47)$$

Air-gap magnetic flux density B0r at no-load operation

$$B_{0r} = \frac{B_{rem}}{k_{\sigma M} + \mu_{rec} k_C \frac{C_\Phi}{C_p}} \quad (3.50)$$

3.3.2. Analysis of the choice of non-commercial vehicle type

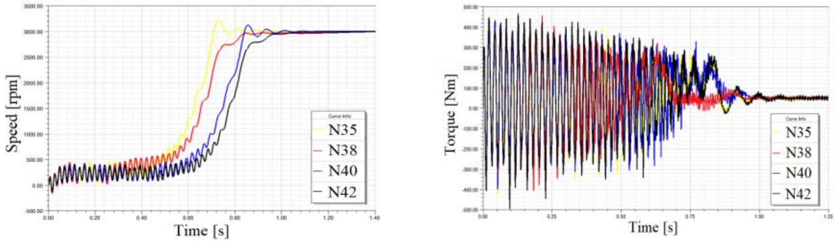

Figure 3.31. Starting and torque characteristics of the Ex-LSPMSM.

Table 3.12. Calculated results for current and back electromotive force characteristics.

Type	t_{trans} (s)	I_{max} (A)	THD_i (%)	E_{1NB} (V)	ΔE (%)
N35	0,90	308	17,8	389	+2,3
N38	0,95	314	16,1	400	+5,2
N40	0,80	312	14,3	410	+7,1
N42	0,85	337	17,6	420	+10,5

* Observation: The results indicate that using N38 and N40 magnets yields quite similar outcomes, with no significant difference between them. However, N40 magnets are more expensive than N38 magnets. Therefore, the use of N38 magnets is considered suitable for the 160 mm Ex-LSPMSM motor in this dissertation.

3.4. Conclusions

Chapter 3 presents a systematic and comprehensive analysis of the demagnetization effects on the operation of explosion-proof line-start permanent magnet synchronous motors (Ex-LSPMSM). It combines theoretical analysis, finite element simulation, and data evaluation to determine how magnet geometric parameters influence the motor's magnetization state and synchronization capability.

First, the chapter analyzes the demagnetization characteristics of NdFeB-N38 magnet material using BH and JH demagnetization curves, clarifying the role of the knee point in defining the safe operating region. At 20°C, the material's knee point is approximately 0.05 T, whereas at 60°C it rises to roughly 0.3 T, demonstrating that the rotor's operating temperature directly affects the magnet's magnetic retention capability.

Simultaneously, the starting current significantly impacts permanent magnet demagnetization. Chapter 3 analyzes the potential for asymmetric demagnetization during Ex-LSPMSM startup, as well as the influence of demagnetization phenomena on motor operation. Based on this, limiting conditions for magnet thickness and width are established to prevent demagnetization. Electromagnetic field simulation results indicate that the magnet width (W_M) significantly affects air-gap flux distribution and the likelihood of demagnetization.

Based on the results of theoretical analysis and verification through simulation results, appropriate permanent magnet parameters have been selected. To avoid the occurrence of demagnetization, the selected permanent magnet thickness is l_M = 9 mm. To ensure the excitation flux generated by the permanent magnets, the selected permanent magnet width is W_M = 33 mm, and the selected permanent magnet grade is N38

CHAPTER 4. EXPERIMENTATION AND RESULTS EVALUATION

4.1. Manufacturing and assembly of Ex-LSPMSM motors

4.2. Experimental model

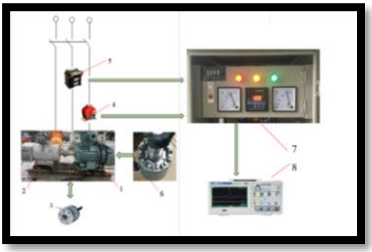

Figure 4.2. Laboratory test model

4.3. Experimental results

Figure 4.3. Current characteristics

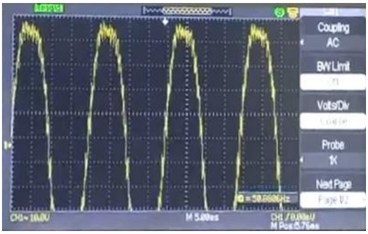

Figure 4.4. Electromotive force measurement results

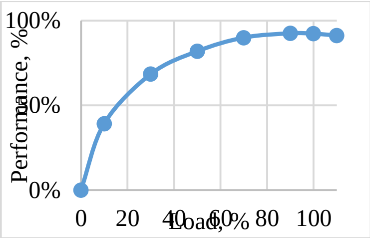

Figure 4.5. Performance characteristics of the Ex-LSPMSM

Table 4.3. Comparison of experimental results I, EMF, and η

No.	Value		Simu l- ation	Experi -ment	Erro r (%)
1	I	(A)	26,2	25,4	3,1
2	EM F	(V)	365,5	357,9	2,1
3	η	(%)	96,6	92,9	3,8

4.4. Conclusions

Chapter 4 details the fabrication and testing of a 15 kW, 3,000 rpm Ex-LSPMSM, based on the rotor design selected in previous chapters. Experimental results demonstrate stable motor operation; the steady-state current waveform is nearly sinusoidal, the no-load electromotive force (EMF) is close to a sine wave, and high efficiency is achieved in the near-rated load range.

Quantitatively, the experimental results show a current amplitude of 25.4 A, which is lower than the simulated value of 26.2 A (a 3.1% discrepancy). The back-EMF amplitude reached 357.9 V, representing a 2.1% difference. Furthermore, the current and back-EMF waveforms exhibit harmonic components consistent with simulation predictions. Testing also confirmed a motor efficiency of 92.9% (a 3.8% discrepancy) compared to the 96.6% obtained in simulation; this variance is attributable to manufacturing processes and measurement factors

CONCLUSIONS AND RECOMMENDATIONS

1. Conclusions

The dissertation systematically investigates a line-start permanent magnet synchronous motor (LSPMSM) with a rated speed of 3,000 rpm and a power output of 15 kW, intended for driving fans and water pumps in underground mining operations. Based on a review of domestic and international research, the dissertation identifies a research gap regarding medium-power, high-speed LSPMSMs that require reliable operation and suitability for the harsh working conditions of the Vietnamese mining industry.

The dissertation systematically studies motors with a shaft center height of 160 mm in general, focusing specifically on the 3K160M-2 (15 kW) Ex-LSPMSM model, with the aim of applying it to fan and water pump loads in underground mining.

The dissertation focuses on addressing the following issues:

- It investigates various design options regarding the number and arrangement of PM bars (2, 3, and 4-bar configurations) and rotor slot structures—specifically comparing designs with and without magnetic bridges. Research results indicate that a 3-bar PM rotor configuration without magnetic bridges is the most suitable, offering a short synchronization time (t_s = 0.45 s), low torque ripple (RipT = 23.1%), low total harmonic distortion of current (THDi = 14.3%), and high efficiency (η = 93.3%).

- It analyzes the demagnetization characteristics of the permanent magnets and determines the conditions required to prevent demagnetization. Based on this analysis, the optimal dimensions for fabrication were determined to be 35x33x9 mm, using N38-grade magnets for the Ex-LSPMSM prototype.

Based on theoretical and simulation results, an experimental Ex-LSPMSM was fabricated and tested in the laboratory. Experimental results show that the motor's current, voltage, and efficiency characteristics align with simulation results, with deviations falling within acceptable limits. The motor achieved a peak efficiency of approximately 92.9% near rated load, validating the research model and demonstrating the practical application potential of the proposed design.

The novel contributions of the dissertation include:

- Proposing a rotor structure featuring three PM bars without magnetic bridges for an Ex-LSPMSM with a 160 mm shaft center height and a speed of 3,000 rpm, suitable for local ventilation fans and water pumps in mining operations.

- Employed a parametric analysis method to optimally select permanent magnet parameters for an Ex-LSPMSM (explosion-proof line-start permanent magnet synchronous motor) with a shaft height of 160 mm and a speed of 3,000 rpm, aiming to improve operating characteristics while accounting for demagnetization conditions.

- Successfully fabricated a prototype 15 kW Ex-LSPMSM in the laboratory for application with local ventilation fans and water pumps in underground mining operations.

AUTHOR'S PUBLISHED WORKS RELATED TO THE DISSERTATION

[1] N. Y. Do, B. T. Trinh (2022), optimizing the design of high performance explosion-proof electric motor used for local fans in underground mines, Mining Industry Journal, No. 6, pp. 56–62.

[2] N. Y. Do, N. H. Bui, B. T. Trinh, and V. U. Luu (2023), "Techno-economic analysis of using high-efficiency motors in mining operations," Industry and Trade Journal, no. 50 (February), pp. 32–34.

[3] B. T. Trinh, A. T. Le, and N. Y. Do (2023), "Influence of permanent magnet thickness on the starting characteristics of a 3,000 rpm LSPMSM," in *Proc. National Conference on Mechanical, Electrical and Automation Engineering (MEAE 2023)*, Hanoi, Vietnam, 2023

[4] N. Y. Do, B. T. Trinh, D. H. Bui, and A. T. Le (2023) , "Investigation of the influence of demagnetization on the steady-state operating characteristics of a two-pole, 15 kW line-start permanent magnet synchronous motor," in *Proceedings of the National Conference on Mechanical, Electrical and Automation Engineering (MEAE 2023)*, 2023.

[5] Thuy, T. B., Cuong, N. X., Tuan, L. A., Do, N. Y. (2023), Effect of Permanent Magnet Structure on Working Characteristics of LSPMSM 3000 rpm, IOP Conference Series: Earth and Environmental Science, vol. 1275, no. 1, p. 012049.
DOI: https://doi.org/10.1088/1755-1315/1275/1/012049 (Index: Scopus)

[6] Do, N. Y., Thuy, T. B., Tuan, L. A., Cuong, N. X. (2024), Rotor Configuration for Improved Working Characteristics of LSPMSM in Mining Applications, Naukovyi Visnyk Natsionalnoho Hirnychoho Universytetu, no. 3, pp. 79–86. DOI: https://doi.org/10.33271/nvngu/2024-3/079 (Scopus, ESCI (Q3))

[7] Do, N. Y., Ngo, X. C., Le, A. T., Do, A. T., Thuy, T. B. (2024), Analysis of Permanent Magnet Demagnetization during the Starting Process of a Line-start Permanent Magnet Synchronous Motor, Engineering, Technology & Applied Science Research, vol. 14, no. 3. DOI: https://doi.org/10.48084/etasr.8576 (Scopus (Q2))

[8] Thuy, T. B., Cuong, N. X., Tuan, L. A., Do, N. Y. (2024), Influence of the NdFeB Permanent Magnet on Working Characteristics of LSPMSM, International Conference on Engineering Research and Applications (ICERA), Springer Proceedings. (Scopus (Q4))

[9] Le Anh, T., Do Nhu, Y., Trinh Bien, T., & Nguyen Van, H. (2024). Studying on current and speed characteristics of LSPMSM of 15 kW, two-pole under remanence reduction of permanent magnets. In Proceedings of the 1st International Conference on Energy, Electronics and Automation (EEA 2024).

[10] Le Anh Tuan, Trinh Bien Thuy, Do Nhu Y (2025), "Parametric analysis to optimize a tradeoff between the efficiency and demagnetization of LSPMSM". International Journal of Electrical and Computer Engineering (IJECE) 563 Vol. 16, No. 2, April 2026, pp. 563~576 ISSN: 2088-8708, DOI: 10.11591/ijece.v16i2.pp563-576.